Heteropolyacids and sulfonic acid-bifunctionalized organosilica spheres for efficient manufacture of cellulose acetate propionate with high viscosity

Huaiying Zhang[a], Lifu Wu[a], Yanfen Zhang[a], Sai An*[a], Haralampos N. Miras*[b], Yu-Fei Song*[a]

[a]*State Key Laboratory of Chemical Resource Engineering, Beijing Advanced Innovation Center for Soft Matter Science and Engineering, Beijing University of Chemical Technology, Beijing 100029 P. R. China.*

*E-mail: songyf@mail.buct.edu.cn; Fax/Tel: +86 10-64431832.

[b]*WestCHEM, School of Chemistry, University of Glasgow, Glasgow, G12 8QQ, UK.*

Abstract. Cellulose acetate propionate (CAP), a high value-added chemical, is traditionally prepared using H_2SO_4 as catalyst. Replacement of the mineral acids by solid acids is current research focus for green and sustainable production of CAP. Herein, we reported the fabrication of novel solid acid catalyst HPW/Si(Et)Si-Dim-SO_3H (Si(Et)Si = ethyl-bridged organosilica and Dim = dihydroimidazole) by incorporating phosphotungstic acid (HPW) and sulfonic acid-based Brønsted acidic ionic liquids (BILs) onto the organosilica nanospheres of the designed catalyst for efficient manufacture CAP *via* esterification. The results indicated that the as-prepared HPW/Si(Et)Si-Dim-SO_3H with 7.5% HPW loading showed the best catalytic performance at 45 °C in 3 h and the resulting CAP exhibited viscosity of 447 mPa·s, *Mw* of 102882 and *DS* of 2.69. Most importantly, the HPW/Si(Et)Si-Dim-SO_3H exhibited high catalytic stability over six consecutive cycles and the obtained products were stable too with similar *DS*, *Mw* and viscosity. As such, the designed heteropolyacids (HPAs) and sulfonic acid-bifunctionalized heterogeneous catalyst is highly promising for biomass conversion under mild conditions.

Keywords: *Solid acid catalyst, Heteropolyacids, Cellulose acetate propionate, High viscosity*

Graphic abstract

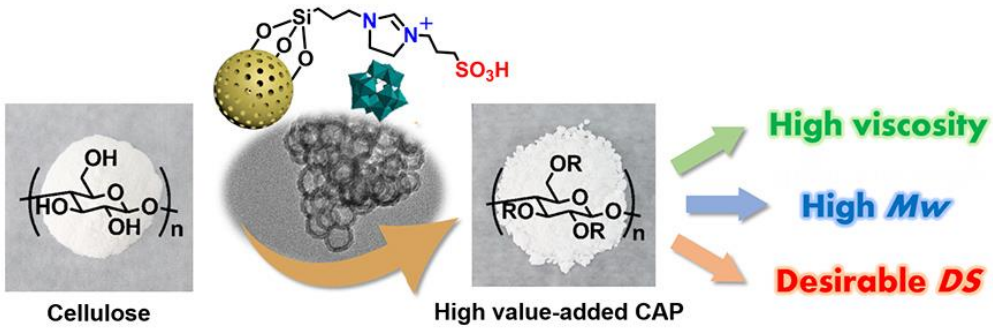

Introduction

Utilization of biorenewable and biodegradable resource on earth, especially cellulose, which can be considered as an inexhaustible polymeric material with fascinating structure and properties, has attracted great attention due to the declining fossil fuel reserves, energy and materials security, and global climate change (Klemm *et al.* 2005; Chen *et al.* 2018; Su *et al.* 2014). Cellulose can be used as a chemical raw material to produce various important cellulose derivatives by esterification, hydrolysis, etherification *etc*. (Heinze *et al.* 2001). One interesting option is the acid-catalyzed esterification of cellulose to produce cellulose acetate propionate (CAP), in which some hydroxyl groups are substituted with acetyl and propionyl groups. Comparing with cellulose acetate (CA), CAP maintains the advantages of excellent transparency and strength, and the incorporation of propionyl groups endows CAP with the properties of water resistance, solubility and compatibility with other polymers. CAP, especially that with high viscosity is considered as high value-added chemicals for specialty coatings, plastic products, tool handles, separation membranes *etc.* (Edgar *et al.* 2001; Li *et al.* 2012). Therefore, the parameters such as the degree of substitution (*DS*), molecular weight (*Mw*), viscosity *etc.* are the important features for evaluating the performance of cellulose esterification, rather than that of traditional conversion or selectivity or yield. For practical purposes, the viscosity and *Mw* of CAP even should be more concerned compared to *DS*. Indeed, H_2SO_4 can effectively catalyze cellulose esterification. Nevertheless, such process suffers from severe corrosion, cellulose degradation and decomposition and uncontrollable process problems (Yan *et al.* 2009). As such, it is imperative to develop environmentally benign catalytic process for cellulose esterification. To date, considerable efforts have been paid and various solvents systems and heterogeneous catalysts were applied for the cellulose esterification. According to the reported work, the explored solvents systems can be beneficial to the dissolution of cellulose such as *N,N'*-dimethylacetamide/LiCl (El Seoud *et al.* 2000; Marson *et al.* 1999), 4-methylmorpholine-*N*-oxide (Biganska *et al.* 2005), tetrabutylammonium fluoride trihydrate/DMSO (Heinze *et al.* 2000; Hussain *et al.* 2004) and ionic liquids (Barthel *et al.* 2006; Huang *et al.* 2011; Köhler *et al.* 2007; Wu *et al.* 2004; Abbott *et al.* 2005; Cao *et al.* 2007, 2009). Besides, several sulfated metal oxides like SO_4^{2-}/ZrO_2 (Yan *et al.* 2006) and SO_4^{2-}/TiO_2 (Meng *et*

al. 2017) were employed for the synthesis of cellulose ester due to their strong acidity. However, the industrial processing and practical applications of CAP is greatly restricted by these catalytic systems because it is really challenging to obtain the CAP with high viscosity and *Mw etc*.

Heteropolyacids (HPAs) are a class of discrete anionic metal oxides with attractive properties (Song *et al.* 2012; Omwoma *et al.* 2014; An *et al.* 2019). They have been regarded as the potential green alternatives to traditional mineral acids owing to their tunable Brønsted or Lewis acidity, thermal stability, redox properties, *etc.* (Tao *et al.* 2015, 2017; Li *et al.* 2016; Shi *et al.* 2017; Li *et al.* 2017; Zhang *et al.* 2019; Fan *et al.* 2013). For instance, cellulose acetate with *DS* of *ca.* 2.2 can be obtained by phosphotungstic acid-catalyzed esterification of cellulose with acetic anhydride in dichloromethane (Fan *et al.* 2013). However, it is still a high challenge in extensive application of HPAs due to the problems of their low BET surface areas (< 10 m^2 g^{-1}), difficult recovery and separation. Tightening environmental legislation is driving the chemical industries to manufacture high value-added CAP by developing efficient and environmental-benign solid acid catalyst.

Under such circumstances, aiming at development of green and sustainable cellulose esterification process, we herein reported a series of heterogeneous catalysts by immobilizing HPW and sulfonic acid-based BILs on organosilica nanospheres (donated as HPW/Si(Et)Si-Dim-SO_3H). The as-prepared HPW/Si(Et)Si-Dim-SO_3H exhibited much higher viscosity and *Mw* compared with H_2SO_4 *etc.* under the same reaction.

Experimental section

Chemical and reagents. 1,2-Bis(trimethoxysilyl)ethane (BTMSE, 97%), Pluronic P123 ($EO_{20}PO_{70}EO_{20}$) and Pluronic F127 ($EO_{106}PO_{70}EO_{106}$) were purchased from Sigma-Aldrich Company Ltd. 1,3,5-trimethylbenzene (TMB) was obtained from Tianjin Guangfu Fine Chemical Research Institute. *N*-[3-(triethoxysilyl)propyl]-4,5-dihydroimidazole (98%) and 1,3-propanesultone (98%) were purchased from Sigma-Aldrich. Phosphotungstic acid (HPW), phosphomolybdic acid (HPMo), silicotungstic acid (HSiW) and silicomolybdic acid (HSiMo) were purchased from Tianjin Fuchen Chemical Reagent Factory.

Ethanol, toluene, acetone, hydrochloric acid, acetic acid and propionic acid were obtained from Beijing Chemical Works. Acetic anhydride and propionic anhydride were purchased from Sinopharm Chemical Reagent Co., Ltd., and microcrystalline cellulose was obtained from Alfa Aesar.

All chemicals were analytical reagent grade. Anhydrous toluene was obtained by treating toluene with sodium, and the other chemicals were directly used without purification.

Preparation of HPW/Si(Et)Si-Dim-SO$_3$H. The synthesized method of mesoporous organosilica nanospheres was referenced to the literature (An *et al.* 2016). Typically, P123 (0.25 g), F127 (0.10 g), HCl (2.20 mL), and TMB (0.70 mL) were successively added into deionized water (12.90 mL) with stirring at room temperature for 2 h. After heated to 40 ^{o}C, BTMSE (0.61 mL) was added dropwise into the mixture and pre-hydrolyzed for 45 min. Then, *N*-[3-(triethoxysilyl)propyl]-4,5-dihydroimidazole (0.14 mL) was added to the mixture with stirring for 24 h and aged at 100 ^{o}C for another 24 h. The obtained suspension was separated by filtration and drying. Then, the solid was dispersed in ethanol (50 mL) and refluxed at 80 ^{o}C for 6 h for three times and drying overnight to remove the template. Subsequently, the obtained solid was dispersed with 1,3-propanesultone (0.27 mL) in anhydrous toluene (30 mL) and refluxed at 80 ^{o}C for 24 h. The solid named Si(Et)Si-Dim^{+}-SO$_3^{-}$ was obtained followed by separation, washing with ethanol and acetone and drying. Finally, the as-prepared Si(Et)Si-Dim^{+}-SO$_3^{-}$ and HPW (0.085 g) were added into deionized water (50 mL) with stirring at room temperature for 12 h. HPW/Si(Et)Si-Dim-SO$_3$H was successfully fabricated followed by separation, washing with water and drying.

Preparation of HPAs/Si(Et)Si-Dim-SO$_3$H. In order to investigate the influence of the composition of Keggin type HPAs on catalytic performance, we prepared HPMo/Si(Et)Si-Dim-SO$_3$H, HSiW/Si(Et)Si-Dim-SO$_3$H and HSiMo/Si(Et)Si-Dim-SO$_3$H by a similar procedure as the above HPW/Si(Et)Si-Dim-SO$_3$H except that HPMo, HSiW and HSiMo were used instead of HPW.

Preparation of HPW/Si(Et)Si-Dim-SO$_3$H-3D$_{int}$. In order to investigate the influence of the morphological characteristics on catalytic performance, the counterpart with 3D interconnected mesostructure (HPW/Si(Et)Si-Dim-SO$_3$H-3D$_{int}$) was prepared by a similar procedure as the above HPW/Si(Et)Si-Dim-SO$_3$H except the molar ratio of composition. The molar ratio of P123 : HCl : BTMSE :

N-[3-(triethoxysilyl)propyl]-4,5-dihydroimidazole : 1,3-propanesultone : HPW = 86 : 3600 : 2409 : 520 : 3054 : 30.

Catalytic tests. The esterification of cellulose to synthesis CAP was carried out in a round-bottom flask in a temperature-controlled oil bath. As shown in Scheme 1, the procedure for esterification of cellulose (2 g, 12.5 mmol) to synthesis CAP suffered from activation by acetic acid (10 g, 167 mmol) and propionic acid (10 g, 135 mmol) at room temperature for 1 h firstly. Then, the esterifying agent acetic anhydride (10 g, 100 mmol) and propionic anhydride (10 g, 75 mmol) were added consecutively into the activated cellulose, followed by the as-prepared catalyst (25 mg). The reaction mixture was keeping in stirring at 45 ^{o}C for 3 h to complete the esterification. Subsequently, the reaction mixture was centrifuged and filtered to obtain viscous CAP solution and recovered catalyst. Finally, the CAP was gradually precipitated by dropping the above viscous liquid into 5-flod deionized water and was collected followed by filtering, washing and drying overnight.

For the study of reusability and the characterization of used-catalyst after each catalytic cycle, the separated catalyst powder was collected by washing with acetone and deionized water and drying overnight, followed by using in another catalytic cycle.

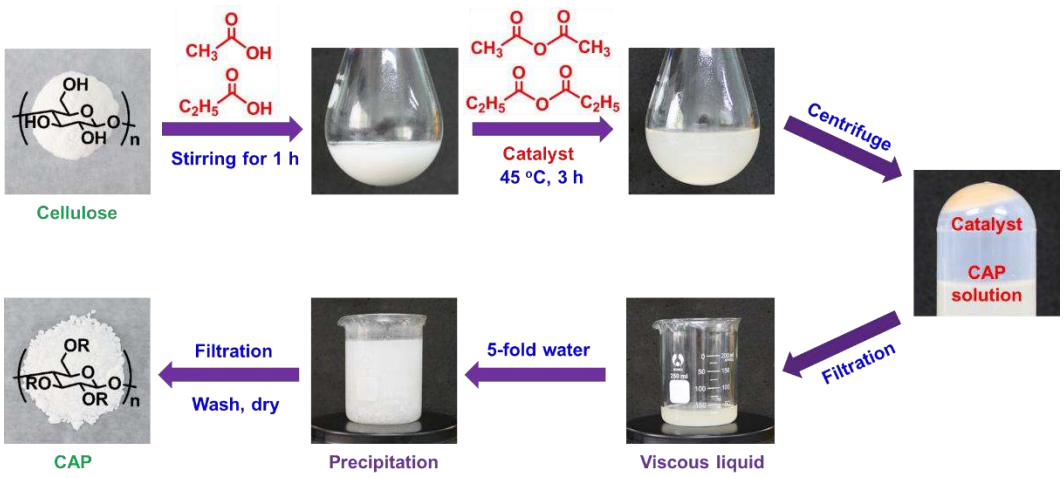

Scheme 1 Illustration for the procedure of esterification of cellulose to CAP

The degree of substitution (*DS*) of CAP were determined by ^{1}H NMR spectra at room temperature. The samples were dissolved in $CDCl_3$, containing a drop of deuterated trifluoroacetic acid to shift active hydrogen to low field area. The *DS* of CAP was calculated using the following equations according to the literature method: (Huang *et al.* 2011)

$$DS_A = \frac{I_A \times 7}{I_{AGU} \times 3} \quad (1)$$

$$DS_P = \frac{I_P \times 7}{\mathrm{I_{AGU}} \times 3} \quad (2)$$

$$DS_{total} = DS_A + DS_P \quad (3)$$

$$A\% = \frac{DS_A \times 43}{162 - DS_{total} + DS_A \times 43 + DS_P \times 57} \times 100\% \quad (4)$$

$$P\% = \frac{DS_P \times 57}{162 - DS_{total} + DS_A \times 43 + DS_P \times 57} \times 100\% \quad (5)$$

where DS_A, DS_P, and DS_{total} are the degree of substitution of acetyl, propionyl and total acyl groups, respectively. I_A, I_P, and I_{AGU} are the peak integrals of the methyl protons of the acetyl (δ 2.0, 3H) and propionyl (δ 1.0, 3H), and all protons of the anhydroglucose unit (AGU) (δ 2.8–5.9, 7H), respectively.

For viscosity measurement, 2.0 g of CAP was added into acetone (8.0 g) to dissolve the sample. The viscosity was determined in water-bath at 25 °C.

Characterization. Transmission electron microscopy (TEM) and high-resolution transmission electron microscopy (HRTEM) observations were performed on a Hitachi H-800 instrument and a JEOL JEM-2010 electron microscope operating at 400 kV, respectively. The N_2 adsorption-desorption measurements were performed on a Micromeritics ASAP 2020M surface area and porosity analyzer after the samples were degassed under vacuum at 100 °C for 6 h before measurements. Fourier transform infrared (FT-IR) spectra were collected on a Bruker Vector 22 infrared spectrometer using the KBr pellet method. X-ray photoelectron spectroscopy (XPS) measurements were recorded with monochromatized ALK exciting X-radiation (PHI Quantera SXM). The solid-state NMR experiments were performed on a Bruker Avance 300M solid-state spectrometer equipped with a commercial 5 mm MAS NMR probe. Thermogravimetric (TG) analysis was tested by an STA-449C Jupiter (HCT-2 Corporation, China) under air atmosphere (20 mL min^{-1}) with a heating rate of 10 °C min^{-1}. HPW loading was determined by inductively coupled plasma atomic emission spectroscopy (ICP-AES) analysis that carried out on a Shimadzu ICPS-7500 instrument. The acid concentrations were tested by acid-base titration. The initial electrode potential (E_i) was determined by SNR B639073181 (Mettler Toledo), with DGi115-SG electrode. ^1H and ^{13}C NMR spectra of the CAP were

collected on a Bruker AV400 NMR spectrometer at 400 MHz. Heteronuclear singular quantum (HSQC) and heteronuclear multiple bond correlation (HMBC) 2D NMR spectra were acquired on a Bruker AV600 NMR spectrometer at 600 MHz. The *Mw* of CAP were determined by Gel permeation chromatography (GPC) analysis, which was performed with 515 HPLC pump and 2410 RI Detector (Waters Corporation, America) with tetrahydrofuran as the mobile phase. The dynamic viscosity of CAP was measured with the NDJ-79 type of rotating viscometer (Shanghai Changji Geological Instrument Co., Ltd).

Result and discussion

Preparation of catalysts. Taking the advantages of controllable morphological nanostructure, excellent surface physicochemical properties and functional diversity of organosilica (Zhang *et al.* 2014; Hu *et al.* 2011; Song *et al.* 2016), we fabricated organosilica-based nanospheres to provide large surface area for incorporating more exposed acid sites. Moreover, the introduced sulfonic acid-based BILs was contributed to increase compatibility and accessibility between catalysts and substrates, and the incorporation of HPW is beneficial for the controllable esterification process, which was expected to facilitate the esterification.

The procedure for preparation of the HPAs and sulfonic acid-bifunctionalized organosilica nanospheres (HPAs/Si(Et)Si-Dim-SO_3H) is shown in Scheme 2, which can be divided into three processes including formation of micelles, co-hydrolysis and -condensation of precursors as well as immobilization of active species. During the first process, the micelles of the triblock copolymer surfactant self-assembled to form spherical topography by using TMB as expansion agent through hydrophilic-hydrophobic interactions. The hydrophobic $–CH_2(CH_3)CHO$ blocks aggregated with hydrophobic TMB together to form a core, while the hydrophilic $–CH_2CH_2O$ blocks are closed to water molecule to formed the hydrated corona. Subsequently, the silica/carbon frameworks gradually formed and the dihydroimidazole modified on organosilica through the co-hydrolysis and co-condensation (An *et al.* 2016). For the immobilization of active species, HPW was successfully incorporated by the strong electrostatic

interaction between anion of HPW and N^+ of the zwitterionic structure (N^+–$(CH_3)_3$–SO_3^-).

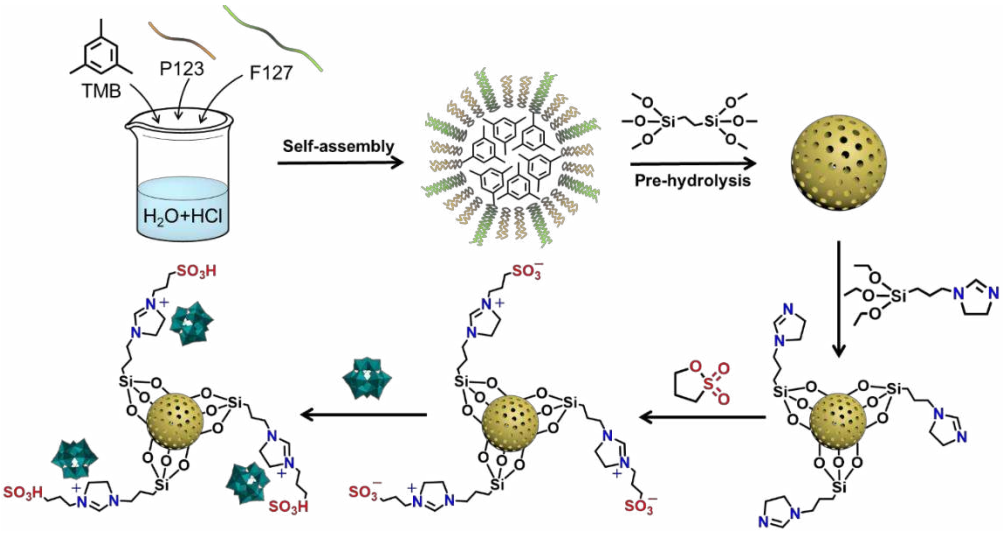

Scheme 2 Illustration of the employed synthetic procedure for the preparation of HPW/Si(Et)Si-Dim-SO_3H

Chemical structure. The structural integrity of the as-prepared HPW/Si(Et)Si-Dim-SO_3H catalysts were confirmed by FT-IR (Figure 1a), W 4*f* XPS (Figure 1b), ^{31}P (Figure 1c) and ^{29}Si MAS NMR (Figure 1d).

As shown in FT-IR spectra (Figure 1a), HPW/Si(Et)Si-Dim-SO_3H and Si(Et)Si exhibit the characteristic bands at 1024, 1107 and 2930 cm^{-1}, which could be assigned to the stretch vibrations of Si–O, Si–C and C–H bond of –CH_2–CH_2– group, respectively (Zhu *et al.* 2011). It is indicated that the FT-IR spectrum of HPW/Si(Et)Si-Dim-SO_3H has the characteristic S–O vibrations at 610 and 530 cm^{-1}, respectively, indicating the existence of −SO_3H group (Cao *et al.* 2018). Moreover, $H_3PW_{12}O_{40}$ shows the characteristic vibration at 1079, 985, 890 and 795 cm^{-1}, respectively, which can be assigned to the stretching of tetrahedral P–O bonds, terminal W=O_t bonds and two types of bending vibrations originating from the bridging W–O_b–W bonds (Schnee *et al.* 2017). The above characteristic vibrational signals can be observed in the FT-IR spectra of HPW/Si(Et)Si-Dim-SO_3H. The above results indicate that 1) the bridged ethyl organosilica, sulfonic acid-based BILs and HPW were successfully incorporated onto the nanospheres; 2) the primary Keggin structure remained intact after immobilization.

In the W 4*f* XPS spectrum of HPW/Si(Et)Si-Dim-SO_3H (Figure 1b), it can be deconvoluted into two signals centered at 37.7 and 35.6 eV due to the W $4f_{5/2}$ and W $4f_{7/2}$ spin-orbit components accordingly (Geng *et al.* 2018). As can be seen

from the ^{31}P MAS NMR spectrum (Figure 1c), the sharp peak centered at –15.2 ppm can be assigned to the resonance of the encapsulated PO_4^{3-} units within the $H_3PW_{12}O_{40}$ cage, indicating the structural integrity of the incorporated $H_3PW_{12}O_{40}$ (Kozhevnikov *et al.* 1996). Another peak at –13.2 ppm indicates the presence of $(\equiv SiOH^{2+})(H_2PW_{12}O_{40}^{-})$ species, which comes from the interaction between HPW and the –OH groups of silica/carbon framework (Kozhevnikov *et al.* 1996; Lefebvre 1992; Kasztelan *et al.* 1990).

As shown in Figure 1d, the ^{29}Si MAS NMR spectrum displays two peaks corresponding to T^3 (δ = –64.7 ppm) and T^2 (δ = –58.4 ppm), where T^m = $RSi(OSi)m(OH)_{3-m}$ (m = 1–3). Most importantly, there are no signals corresponding to the Q^n species, where Q^n = $Si(OSi)_n(OH)_{4-n}$, (n = 2–4), confirming that the integrity of silica/carbon framework (Inagaki *et al.* 1999, 2002).

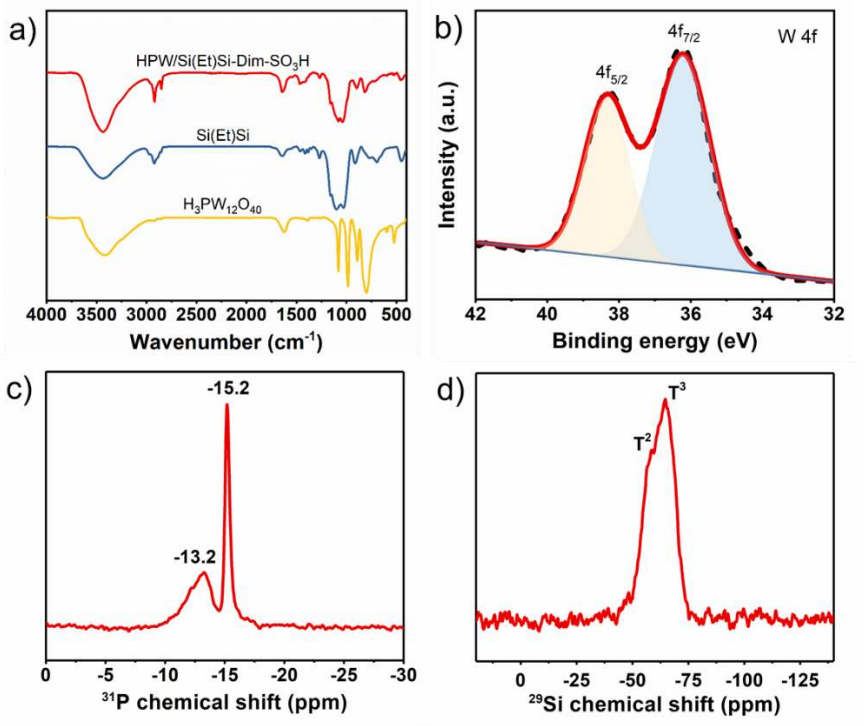

Figure 1 FT-IR spectra of HPW/Si(Et)Si-Dim-SO_3H, Si(Et)Si and $H_3PW_{12}O_{40}$ (a); XPS spectrum for the W 4*f* core level (b), ^{31}P (c) and ^{29}Si (d) MAS NMR of HPW/Si(Et)Si-Dim-SO_3H

The thermogravimetric studies were carried out in the range of 30 to 800 °C. As shown in Figure S1, the TG-DTA plot of HPW/Si(Et)Si-Dim-SO_3H shows two consecutive weight losses. The first weight loss occurs in the range of 30 to 100 °C (*ca.* 3.84%) which can be attributed to the loss of water molecules adsorbed by the catalysts. Another weight loss in the range of 200 to 600 °C (*ca.* 19.58%) can be attributed to the decomposition of the bridging ethyl groups, sulfonic acid-

based BILs, residual P123, F127 and the collapse of the silica/carbon framework and decomposition of the Keggin structure.

Based on the above structural information, we successfully fabricated the HPAs and sulfonic acid-bifunctionalized organosilica nanospheres and they are stable below 200 °C.

Morphology, porosity and acidity. TEM images of as-prepared catalysts (Figure 2) indicates that they are composed of well-dispersed nanospheres with uniform particle size. It shows that the particle size and inner diameter of HPW/Si(Et)Si-Dim-SO_3H are *ca.* 32 nm and *ca.* 17 nm, respectively, and the shell thickness is *ca.* 7 nm (Figure 2a). Comparing with Si(Et)Si-Dim-SO_3H, HPW/Si(Et)Si-Dim-SO_3H **1** and HPW/Si(Et)Si-Dim-SO_3H **2** (Figure S2), which possess different HPW loading, the spherical nanostructure is still remained, indicating that nanospheres formed by P123- and F127-directed route is stable enough. From HRTEM images of HPW/Si(Et)Si-Dim-SO_3H (Figure 2b and 2c), we can clearly see complete and well-defined nanospheres with uniformly dispersed black spots of 1–2 nm, which is in agreement with the dimensions of the $H_3PW_{12}O_{40}$ clusters (yellow circles in Figure 2c). Furthermore, Figure 2d shows the EDS isotherm of HPW/Si(Et)Si-Dim-SO_3H, which confirms the presence of HPW. The above results suggest that the HPW were successfully incorporated to the silica/carbon framework.

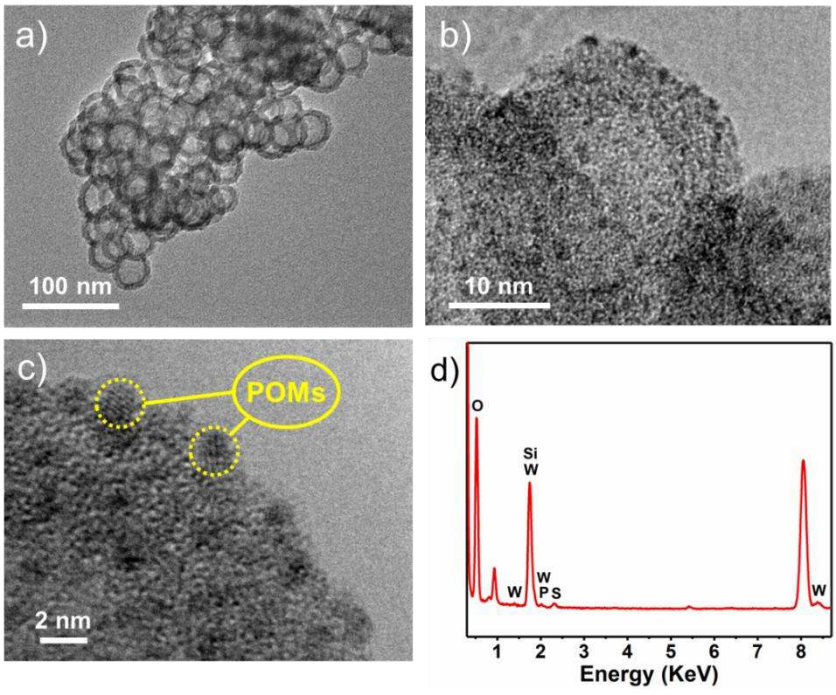

Figure 2 TEM images (a), HRTEM images (b, c) and EDS isotherm (d) of HPW/Si(Et)Si-Dim-SO_3H

Figure 3a shows the N_2 adsorption-desorption isotherms, in which the type IV isotherm confirms the mesoporous nature of the HPW/Si(Et)Si-Dim-SO_3H and Si(Et)Si. Moreover, both of them exhibit one hysteresis loop that can be attributed to the hollow interior of the spherical nanostructures or the void space formed between the loosely packed spheres. The capillary condensation steps occur at P/P_0 = 0.45−0.99. As shown in Figure 3b, BJH pore size distribution curves show that the HPW/Si(Et)Si-Dim-SO_3H and Si(Et)Si exhibit one peak at 15.6 nm and 15.8 nm, respectively, which confirms the mesoporous structure of the nanospheres and corresponds to the uniform hollow interior of the nanospheres.

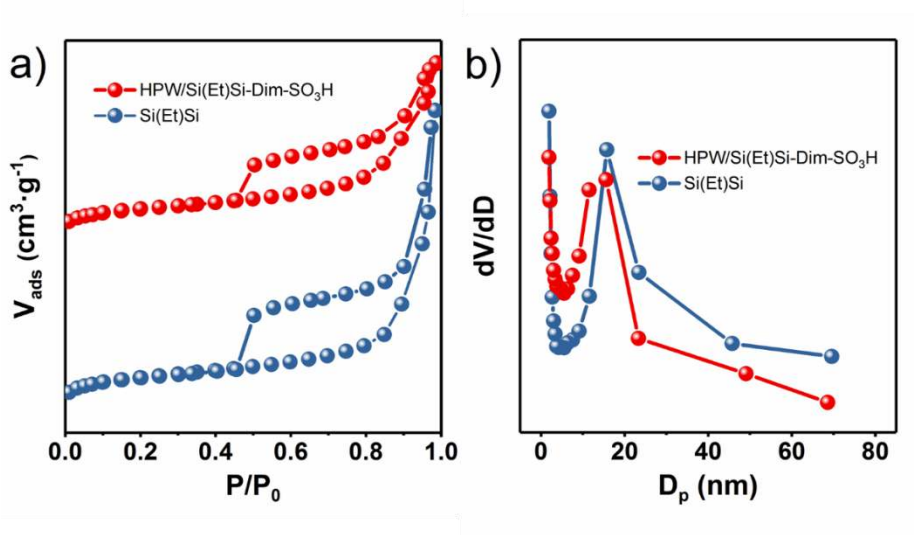

Figure 3 Nitrogen gas adsorption-desorption isotherms (a) and BJH pore size distribution profiles (b) of Si(Et)Si and HPW/Si(Et)Si-Dim-SO_3H

From the detailed textural parameters in Table 1, it can be found that as-prepared catalysts possess similar pore size (15.6 and 15.8 nm), large BET surface area (376 and 439 $m^2\ g^{-1}$) and pore volume (1.11 and 1.95 $cm^3\ g^{-1}$). The as-prepared HPW/Si(Et)Si-Dim-SO_3H exhibits the acid density of 953 μmol g^{-1}. The initial electrode potential (E_i) indicates the maximum acid strength of the surface site. Materials with E_i values higher than 100 mV are defined as very strong solid acids, and that in the range of 0−100 mV can be defined as strong solid acids (Kuzminska *et al.* 2014). It can be seen that HPW/Si(Et)Si-Dim-SO_3H presents 187.7 mV of E_i, which clearly indicates that it possesses strong Brønsted acidity.

Table 1 Porosity and acidity of HPW/Si(Et)Si-Dim-SO_3H and Si(Et)Si

Catalysts	S_{BET} ($m^2\ g^{-1}$)	D_p (nm)	V_p ($cm^3\ g^{-1}$)	*Acid density* (μmol g^{-1})	E_i (mV)
HPW/Si(Et)Si-Dim-SO_3H	376	15.6	1.11	953	187.7

Si(Et)Si	439	15.8	1.95	75	–31.4

Catalytic studies. In order to screen out the HPAs and sulfonic acid-bifunctionalized organosilica nanospheres with the best performance, the influences of the composition and loading of HPAs on the catalytic activity were carefully investigated. The corresponding characteristic results are displayed in Figure S1−S4.

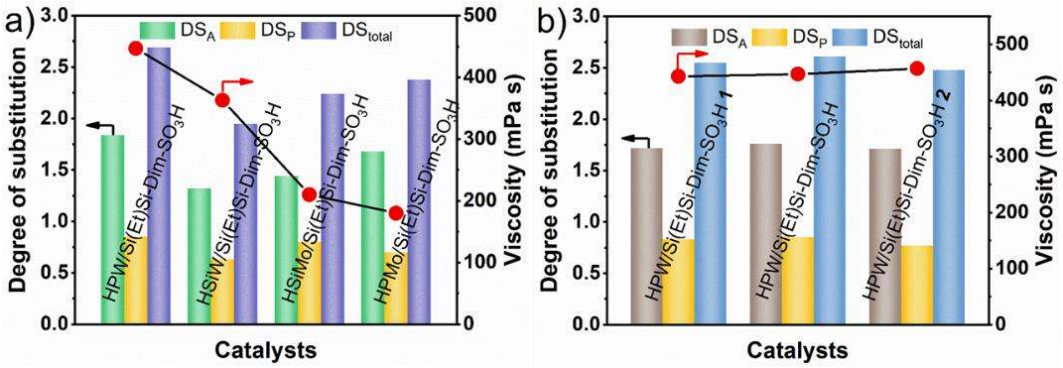

Figure 4 Influence of the composition (a) and loading (b) of HPAs on the *DS* and viscosity of CAP. Reaction conditions: 45 °C, 1.25 wt% catalyst, anhydride/cellulose mass ratio of 10:1 and acetic anhydride/propionic anhydride mass ratio of 1 : 1 for 3 h

The Brønsted acid strength of HPAs is closely related to the composition and the Brønsted acid strength order as follows $H_3PW_{12}O_{40}$ > $H_3PMo_{12}O_{40}$ > $H_4SiW_{12}O_{40}$ > $H_4SiMo_{12}O_{40}$. Therefore, the influence of the composition of Keggin type HPAs on esterification performance was investigated firstly (Figure 4a and Table S1). Among the HPW/Si(Et)Et-Dim-SO_3H, HPMo/Si(Et)Et-Dim-SO_3H, HSiW/Si(Et)Et-Dim-SO_3H and HSiMo/Si(Et)Et-Dim-SO_3H catalysts, the highest *DS* of 2.69, *Mw* of 102882 and viscosity of 447 mPa·s are obtained by HPW/Si(Et)Et-Dim-SO_3H-catalyzed esterification reaction because of the inherent strong acidic strength of HPW. The above results further demonstrate the importance of Brønsted acid strength to the manufacture of CAP with high viscosity.

Subsequently, the influence of HPW loading on CAP properties was evaluated by choosing HPW/Si(Et)Et-Dim-SO_3H **1** (HPW loading of 5.9%), HPW/Si(Et)Et-Dim-SO_3H (HPW loading of 7.5%) and HPW/Si(Et)Et-Dim-SO_3H **2** (HPW loading of 14.2%) as representative catalysts. The results in Figure 4b and Table S1 show that *DS* and *Mw* of CAP slightly increase with increasing the HPW loading, while it decreases with further increasing the HPW loading. Meanwhile, the three products exhibit similar viscosity (*ca.* 443–457 mPa·s).

Based on the above results, the *DS* and *Mw* of CAP strongly linked to the HPW loading and HPW/Si(Et)Et-Dim-SO_3H-catalyzed esterification exhibit the highest *DS* (2.69) and *Mw* (102882). Therefore, HPW/Si(Et)Si-Dim-SO_3H with HPW loading of 7.5% is chosen for subsequent catalytic test.

Considering of the importance of various reaction parameters for high value-added CAP, we carefully investigated the influence of mass ratio and molar ratio of substrates, mass ratio and molar ratio of anhydride, temperature and reaction time on *DS*, viscosity and *Mw* of CAP by choosing the optimized HPW/Si(Et)Si-Dim-SO_3H as the representative catalyst.

First of all, the amount of esterifying agent (acetic anhydride and propionic anhydride), which is crucial to the properties of CAP, were studied. In Figure 5a and Table S2, the *DS*, viscosity and *Mw* gradually increased with increasing anhydride/cellulose mass ratio from 6 : 1 to 10 : 1 (molar ratio from 8.4 : 1 to 14 : 1), and the highest *DS* of 2.69, viscosity of 447 mPa·s and *Mw* of 102882 are obtained. Nevertheless, further increase of the anhydride/cellulose mass ratio to 12 : 1 (molar ratio of 16.8 : 1) and 14 : 1 (molar ratio of 19.6 : 1) leads to the decrease of *DS*, viscosity and *Mw*. Based on the principle of chemical equilibrium, higher anhydride-to-cellulose mass ratio or excessive esterifying agent can drive the equilibrium to the CAP product and thereby higher *DS* and *Mw*. However, much more esterifying agent may dilute the reaction system, leading to the poor properties of CAP. As a result, we select the anhydride and cellulose mass ratio of 10 : 1 (molar ratio of 14 : 1) for the subsequent catalytic tests.

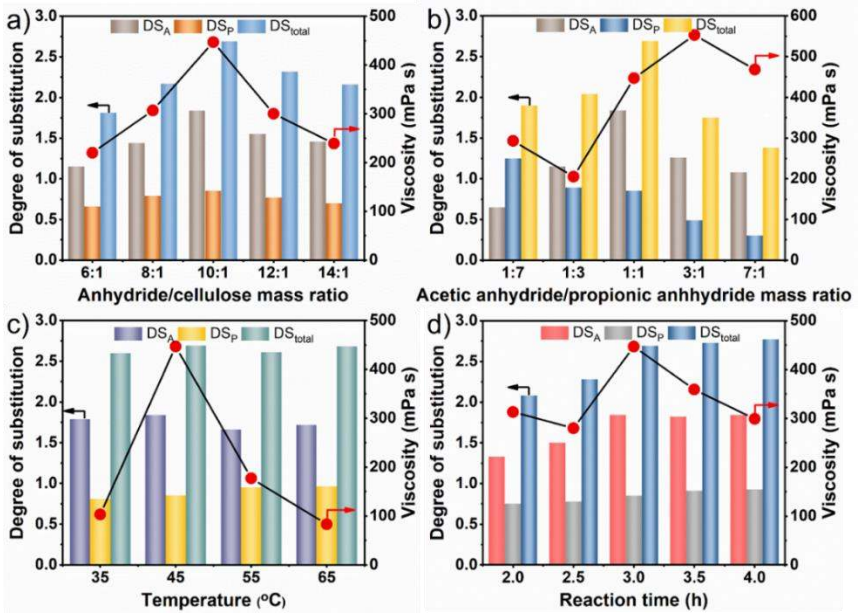

Figure 5 Influence of anhydride/cellulose mass ratio (a), acetic anhydride/propionic anhydride mass ratio (b), temperature (c) and reaction time (d) on the *DS* and viscosity of CAP

Secondly, we controlled acetic anhydride-to-propionic anhydride mass ratio to investigate the corresponding *DS*, *Mw* and viscosity of CAP (Figure 5a and Table S3). It is found that the CAP exhibits desired *DS*, high *Mw* and viscosity only under the acetic anhydride-to-propionic anhydride of 1 : 1 (molar ratio of 4 : 3). Moreover, as shown in Figure 5b, the viscosity of CAP is on the increase with DS_P decreasing, indicating that the content of propionyl groups has a profound influence on the CAP viscosity. Considering of *DS*, *Mw* and viscosity, 1 : 1 of acetic anhydride-to-propionic anhydride (molar ratio of 4 : 3) is selected for the subsequent catalytic tests.

Figure 5c shows the effect of reaction temperature (35, 45, 55 and 65 °C) on *DS* and viscosity of CAP. It is found that there is little difference to the *DS* (2.65−2.69) of CAP with adjusting reaction temperature because of the equilibrium of esterification of cellulose over 45 °C. However, the viscosity highly depends on the reaction temperature. For example, viscosity rises sharply from 103 to 447 mPa·s with the reaction temperature changed from 35 °C to 45 °C. Then, with further increasing reaction temperature to 55 and 65 °C, viscosity drops to 177 and 83 mPa·s, respectively. Additionally, the *Mw* of the products exhibits a similar trend with viscosity (Table S4), and exhibit the highest value of 102882 at 45 °C. This is due to that the glycosidic bonds among cellulose base rings are unstable under high temperature, leading to the degradation of cellulose. Thus, 45 °C was selected for the optimized reaction temperature.

At last, in order to investigate the influence of reaction time on catalytic performance, 2.0, 2.5, 3.0, 3.5, and 4.0 h was selected. As shown in Figure 5c, the *DS* of CAP increases obviously from 2.08 to 2.69 with prolonging reaction time from 2.0 to 3.0 h. Then, it tends to be stable when further prolonging reaction time to 3.5 and 4.0 h. On the other hand, the viscosity shows a rising trend from 2 h to 3 h and drops down to 299 mPa·s with further prolonging time to 4.0 h. This is due to the degradation of long chain in the amorphous cellulose or in the crystalline cellulose with weak intermolecular and intramolecular hydrogen bond under high temperature and acidic system.

On the basis of the above results, the optimized reaction conditions can be determined as following: 10 g acetic anhydride (100 mmol), 10 g propionic

anhydride (75 mmol), with 1.25 wt% catalyst, 45 °C, 3 h for esterification of cellulose to CAP.

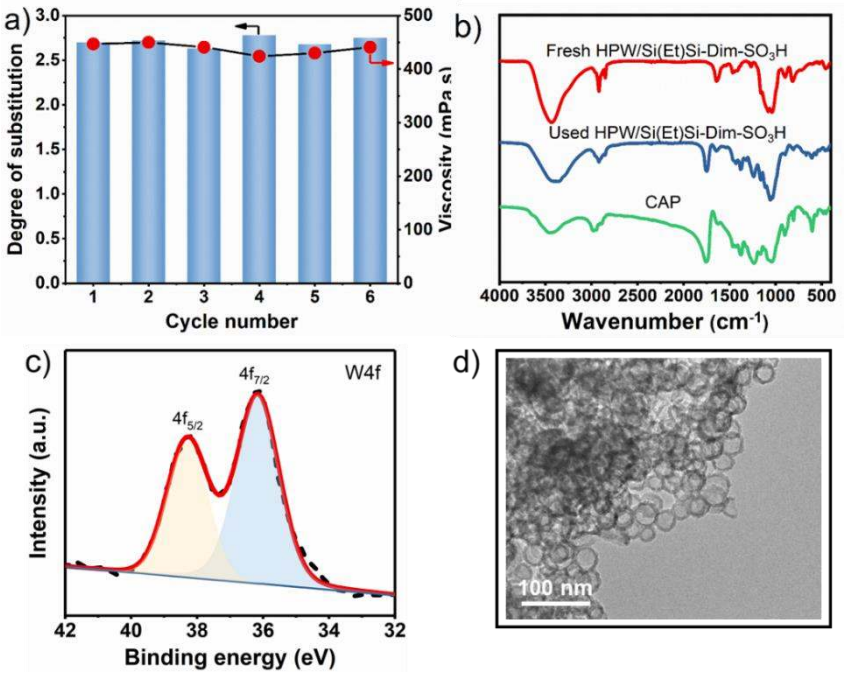

Figure 6 Reusability (a), FT-IR spectra (b), XPS spectrum of W *4f* (c) and TEM image (d) of used HPW/Si(Et)Si-Dim-SO_3H

To evaluate the reusability and stability of the catalytic system, the HPW/Si(Et)Si-Dim-SO_3H catalyze the esterification of cellulose for six consecutive cycles under the optimized reaction condition. After each catalytic cycle, the separated catalyst powder was washed with acetone and deionized water and dried overnight. The details of regenerating treatment of catalysts are shown in Scheme 1. As shown in Figure 6a, the *DS*, *Mw* and viscosity of CAP remain the range of 2.63–2.75, 81634–91530 and 424–450 mPa·s, respectively, after six cycles. In order to identify potential leaching of the HPW into the solution, we conducted ICP-AES analysis to determine the tungsten content of reaction mixture after removing the catalyst at the end of the cycle. The results showed that the concentration of the tungsten in the system is below the detection limit, confirming that there is no detectable leaching of HPW species under this experimental condition. Subsequently, the structure of the used HPW/Si(Et)Si-Dim-SO_3H catalyst was further analyzed. In Figure 6b, the characteristic peaks assigned to the Keggin type HPW and sulfonic acid groups can be still be detected. Additionally, a new peak appears at the spectra of used HPW/Si(Et)Si-Dim-SO_3H, which attributed to the adsorption of CAP on the surface of catalysts. The deconvoluted W 4*f* XPS spectrum reveals again in this case two signals

centered at 38.3 and 36.2 eV (Figure 6c), originating from the contributions of the W $4f_{5/2}$ and W $4f_{7/2}$ spin-orbit components, which found to be similar to the freshly prepared HPW/Si(Et)Si-Dim-SO_3H catalyst. Additionally, TEM image (Figure 6d) exhibits well-defined hollow nanospheres, which indicates that the spherical nanostructure of as-prepared catalysts is retained after recycling. Therefore, the as-prepared HPW/Si(Et)Si-Dim-SO_3H can act as efficient and stable solid acid catalysts with excellent catalytic performance for the esterification reaction of cellulose to yield CAP at least six cycles.

Table 2 Esterification activity and CAP parameters comparison of HPW/Si(Et)Si-Dim-SO_3H with respect to commercial and reference catalysts[a]

Entry	*Catalyst*	*Time* (h)	*Temp.* (°C)	DS_{total}	DS_A	DS_P	*Mw*	*Viscosity* (mPa·s)
1	HPW/Si(Et)Si-Dim-SO_3H	3	45	2.69	1.84	0.85	102882	447
2	HPW/Si(Et)Si-Dim-SO_3H-$3D_{int}$	3	45	2.77	1.91	0.86	91427	298
3	H_2SO_4	3	45	2.97	2.14	0.83	82606	160
4	HPW[b]	3	45	2.58	1.82	0.76	89255	200
5	Amberlyst-15	3	45	2.79	1.99	0.80	103023	237
6	Blank	3	45	—	—	—	—	—
7	PDVB-VBC-IM-PW_{12} (Zhang *et al.* 2019)	3	45	2.77	1.84	0.93	92500	335
8	AmimCl (Huang *et al.* 2011)	5	100	2.67	0.21	2.46	—	—
9	Iodine (Cheng *et al.* 2011)	24	100	2.80	1.60	1.20	—	—
10	DBU/CO_2/DMSO (Xu *et al.* 2018)	2	80	2.72	1.76	0.96	—	—
11	TBAA (Yu *et al.* 2016)	6[c]	65	2.99	1.79	1.20	—	—

Note: PDVB-VBC (copolymer of divinylbenzene with 4-vinylbenzyl chloride); AminiCl (1-allyl-3-methylimidazolium chloride); DBU (1, 8-Diazabicyclo[5.4.0]undec-7-ene); TBAA (tetrabutylammonium acetate). [a]Reaction conditions: 2 g cellulose, 25 mg catalyst, 10 g acetic anhydride, 10 g propionic anhydride for entry 1-7; [b]Equivalent to the weight of HPW on HPW/Si(Et)Si-Dim-SO_3H; [c]Acetic anhydride was added into the reaction system 3 h after propionic anhydride.

Comparing with 3D interconnected mesostructural HPW/Si(Et)Si-Dim-SO_3H-$3D_{int}$ (Table 2, entry 2), spherical HPW/Si(Et)Si-Dim-SO_3H exhibited higher *Mw* (102882) and viscosity (447 mPa s) by a controllable and mild process, which benefited from the large surface with more exposed and accessible acid sites. Furthermore, the prepared HPW/Si(Et)Si-Dim-SO_3H was compared with inorganic acid H_2SO_4, HPW and commercial available Amberlyst-15 under the same reaction conditions (Table 2, entry 3–5). As shown in entry 3 of Table 2, H_2SO_4-catalyzed cellulose esterification performed with considerably fast reaction rate, and the highest *DS* of 2.97, the lowest *Mw* (82606) and viscosity (160 mPa s)

were obtained, which is attributed to the degradation and decomposition of cellulose. As for the others, HPW/Si(Et)Si-Dim-SO_3H obtained CAP with the highest viscosity (447 mPa·s) despite their similar desired *DS* (2.58–2.79) and *Mw* (89255–103023). Moreover, in the absence of any catalysts (Table 2, entry 6), substrate cellulose didn't react with esterifying agent and there is no product CAP can be obtained in the system after completely reaction. Comparing with our previous work (Table 2, entry 7), CAP obtained by HPW/Si(Et)Si-Dim-SO_3H not only maintains excellent properties but also exhibits higher *Mw* (102882), viscosity (447 mPa s) and more controllable esterification process. As shown in entry 8–11 of Table 2, the reported homogeneous system of cellulose esterification always proceed under higher temperature (65–100 ^oC) or even much longer reaction time (*e.g.* 24 h by iodine) than this work. It is worth noting that the HPW/Si(Et)Si-Dim-SO_3H-catalyzed esterification is more controllable to keep *DS* of CAP within 2.4−2.7, which meets the industrial requirements. More importantly, the *Mw* and viscosity are not mentioned in most of reported work, which are the crucial properties of CAP to evaluate whether they are high value-added chemicals. As a consequence, as-prepared HPW/Si(Et)Si-Dim-SO_3H catalyst is competitive in the esterification of cellulose to yield CAP due to the excellent catalytic activity with desired *DS*, high *Mw* and viscosity under mild reaction conditions.

Studies of CAP products. The products obtained by HPW/Si(Et)Si-Dim-SO_3H-catalyzed esterification of cellulose were further characterized by ^1H, ^{13}C NMR spectroscopy (Figure 7a, 7b), HSQC and HMBC 2D NMR spectroscopy (Figure 7c, 7d). As shown in ^1H NMR spectrum of CAP, the peaks at 3.45–5.20 ppm are assigned to the anhydroglucose protons. The peaks at 1.01–1.20 ppm and 2.16–2.44 ppm are attributed to the methyl and methylene groups of propionyl moieties, respectively. Additionally, the signals assigned to methyl of acetyl are observed at 1.88–2.15 ppm (Huang *et al.* 2011). In Figure 7b, the ^{13}C NMR spectrum of the CAP shows signals at 173 and 170 ppm, which are assigned to the carbonyl carbon of propionyl and acetyl groups, respectively. The characteristic signals are attributed to C1, C4, C5, C3, C2 and C6 of anhydroglucose carbonate region appear at 100.5, 76.1, 72.9, 72.5, 71.8 and 62.0 ppm, respectively (Huang *et al.* 2011). The peaks corresponding to the methyl and methylene groups in propionyl can be observed at 9.0 and 27.3 ppm, while the peak centered at 20.4

ppm is assigned to methyl of acetyl. The HSQC spectrum (Figure 7c) shows the connectivity of C−H bond except for the quaternary carbons (C=O of acetyl and propionyl groups). Furthermore, the HMBC spectrum exhibits the correlations between protons of anhydroglucose and carbonyl carbons of acyl. The correlation peaks centered at 4.82×173 ppm, 4.78×170 ppm, 5.10×173 ppm and 5.06×170 ppm confirm that the acetyl and propionyl groups are mostly substituted at C2 and C3.

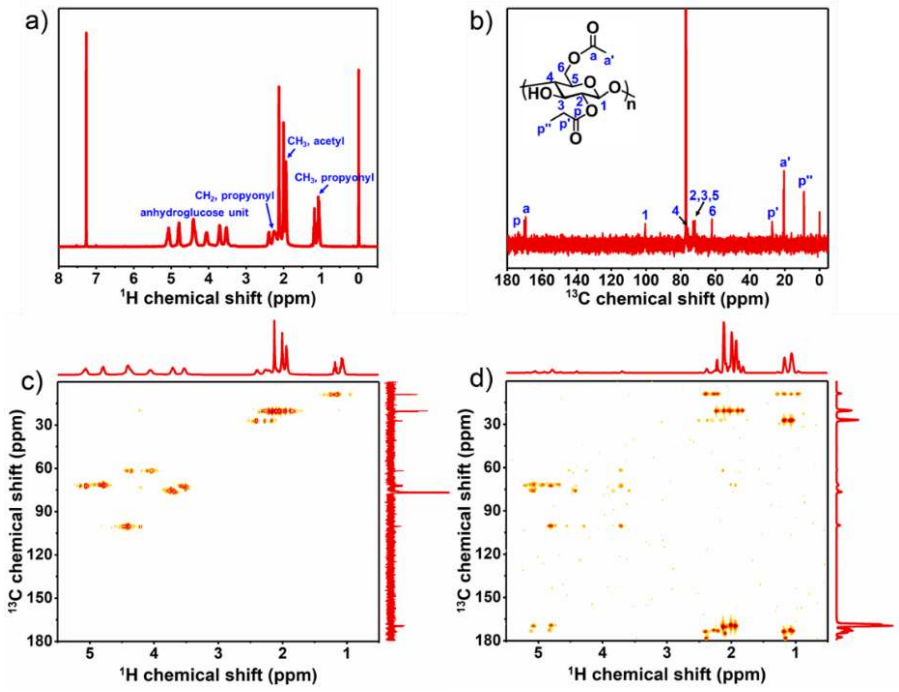

Figure 7 ^{1}H NMR (a), ^{13}C NMR (b) spectra, HSQC (c) and HMBC (d) 2D NMR spectra of CAP

Furthermore, the thermogravimetric studies were carried out in the range of 30 to 600 °C. As shown in Figure S5, the TG-DTA plots show only one weight loss at 367.9 °C for CAP obtained by HPW/Si(Et)Si-Dim-SO_3H-catalyzed cellulose esterification and 334.4 °C for cellulose. It can be seen that it is a rapid decomposition process due to the breakage of intermolecular glycoside and C−C bonds with increasing temperature. Comparing with cellulose, the thermostability of CAP was obviously enhanced due to the incorporation of acetyl and propionyl groups.

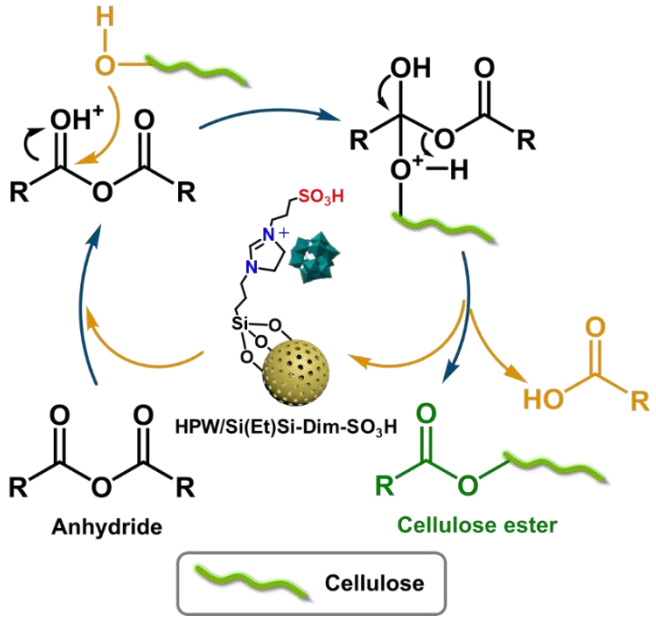

491

492 **Scheme 3** The proposed mechanism of HPW/Si(Et)Si-Dim-SO_3H-catalyzed cellulose
493 esterification

494 ***Mechanism.*** For a typical manufacturing process of CAP, it concludes three
495 parts of cellulose activation, cellulose esterification and separation with catalysts.
496 The strong intermolecular and intramolecular hydrogen bonds presented in
497 cellulose are conducive to forming crystalline regions, hindering small solvent
498 molecules from contacting with the cellulose molecules and thereby reducing the
499 solubility (Yu *et al.* 2016; Wu *et al.* 2004). Therefore, the activation of cellulose is
500 an important step in a typical esterification reaction of cellulose to synthesize
501 CAP. During the process of activation, the crystallinity of cellulose decreased and
502 the structure of amorphous and outermost cellulose was destroyed after the
503 infiltrating of acetic acid and propionic acid. Meanwhile, the accessibility of
504 hydroxyl was improved due to the breakage of the hydrogen bonds between
505 cellulose molecules. It is worth noting that the activation process is a physical
506 swelling process to change the crystalline of cellulose, which not occurs chemical
507 reaction.

508 Taking the HPW/Si(Et)Si-Dim-SO_3H-catalyzed esterification process as an
509 example, the intermolecular and intramolecular hydrogen bonds presented in
510 cellulose were further broken attributed to the incorporation of the sulfonic acid-
511 based BILs in HPW/Si(Et)Si-Dim-SO_3H, which improved the accessibility of
512 hydroxyl groups of cellulose to active sites. Then, the cellulose esterification
513 started from protonation of the carbonyl groups of acetic and propionic anhydride
514 molecules by –SO_3H and HPW active species. During this period, the well-

515 defined spherical nanostructure can provide large BET surface area with more
516 exposed acid sites, which contributes to improving the accessibility of the
517 reactants with active sites. On the other hand, the inherent strong Brønsted acid
518 nature of as-prepared catalysts ensured the reactions proceed at a considerably fast
519 rate. Later, the protonated carbonyl groups were attacked by the hydroxyl groups
520 of cellulose, and the cellulose ester (CAP) was finally obtained followed by the
521 release of carboxylic acid and proton (Scheme 3). Interestingly, the
522 HPW/Si(Et)Si-Dim-SO_3H-catalyzed cellulose esterification was a controllable
523 process to prevent the depolymerization or degradation of cellulose with the
524 incorporation of HPW and sulfonic acid-based BILs, which is benefit to obtain
525 high value-added CAP products.

526 Most importantly, the strong Brønsted acidity of as-prepared catalysts was
527 maintained after the reaction due to the strong electrostatic interaction between the
528 anion of HPW and the N^+ cation of dihydroimidazole and the strong anchoring
529 effect on proton originated from HPW and sulfonic acid-based BILs. Moreover,
530 the loss of proton in as-prepared catalysts could be prevented owing to the acidic
531 reaction system consisted of acetic acid and propionic acid.

532 Conclusion

533 To summarize, a series of heterogeneous catalysts by immobilizing HPW
534 and sulfonic acid-based BILs on organosilica nanospheres (HPW/Si(Et)Si-Dim-
535 SO_3H) were successfully fabricated. The heterogeneous catalysts of the spherical
536 HPW/Si(Et)Si-Dim-SO_3H with 7.5% HPW loading showed excellent catalytic
537 activity in the esterification of cellulose to CAP. As a result, the CAP with *DS* of
538 2.69, viscosity of 447 mPa·s and *Mw* of 102882 was obtained. Such catalytic
539 performance can be assigned to the fact that 1) the well-defined spherical
540 nanostructures provide the large surface area with more exposed acid sites for the
541 HPW/Si(Et)Si-Dim-SO_3H catalyst, which may shorten the mass transfer pathway
542 and thereby improve the accessibility of the reactants with active sites of catalysts;
543 2) the inherent strong Brønsted acid nature of HPW/Si(Et)Si-Dim-SO_3H by
544 incorporating HPW and sulfonic acid-based BILs is beneficial to obtain high
545 value-added CAP.

546 Furthermore, the HPW/Si(Et)Si-Dim-SO_3H catalysts showed excellent
547 stability after six consecutive catalytic cycles without obvious loss of catalytic

activity. Therefore, the HPW/Si(Et)Si-Dim-SO_3H can act as efficient and environmentally benign heterogeneous catalysts for the high-value added CAP production.

Acknowledgements

This research was supported by the National Key Research and Development Program of China (2017YFB0307303), the National Nature Science Foundation of China (21625101, 21521005, 21808011), Postdoctoral Science Foundation of China (2018M631313) and the Fundamental Research Funds for the Central Universities (XK1802-6, XK1803-05, XK1902, 12060093063).

References

Abbott A P, Bell T J, Handa S, Stoddart B (2005) *O*-Acetylation of cellulose and monosaccharides using a zinc based ionic liquid. Green Chem 7: 705–707. https://doi.org/10.1039/B511691K

An S, Sun Y, Song D, Zhang Q, Guo Y, Shang Q (2016) Arenesulfonic acid-functionalized alkyl-bridged organosilica hollow nanospheres for selective esterification of glycerol with lauric acid to glycerol mono- and dilaurate. J Catal 342: 40–54. https://doi.org/10.1016/j.jcat.2016.07.004

An S, Liu J-C, Zhang H, Wu L, Qi B, Song Y-F (2019) Recent progress on the frontiers of polyoxometalates structures and applications. Sci China Chem 62: 159–161. https://doi.org/10.1007/s11426-018-9378-4

Barthel S, Heinze T (2006) Acylation and carbanilation of cellulose in ionic liquids. Green Chem 8: 301–306. https://doi.org/10.1039/B513157J

Biganska O, Navard P (2005) Kinetics of precipitation of cellulose from cellulose−NMMO−water solutions. Biomacromolecules 6: 1948–1953. https://doi.org/10.1021/bm040079q

Cheng H N, Dowd M K, Shogren R L, Biswas A (2011) Conversion of cotton byproducts to mixed cellulose esters. Carbohydr Polym 86: 1130–1136. https://doi.org/10.1016/j.carbpol.2011.06.002

Cao Y, Wu J, Meng T, Zhang J, He J, Li H, Zhang Y (2007) Acetone-soluble cellulose acetates prepared by one-step homogeneous acetylation of cornhusk cellulose in an ionic liquid 1-allyl-3-methylimidazolium chloride (AmimCl). Carbohydr Polym 69: 665–672. https://doi.org/10.1016/j.carbpol.2007.02.001

Cao Y, Wu J, Zhang J, Li H, Zhang Y, He J (2009) Room temperature ionic liquids (RTILs): a new and versatile platform for cellulose processing and derivatization. Chem Eng J 147: 13–21. https://doi.org/10.1016/j.cej.2008.11.011

Cao Z, Zhao X, He F, Zhou Y, Huang K, Zheng A, Tao D (2018) Highly efficient indirect hydration of olefins to alcohols using superacidic polyoxometalate-based ionic hybrids catalysts. Ind Eng Chem Res 57: 6654–6663. https://doi.org/10.1021/acs.iecr.8b00535

583 Chen Z, Zhang J, Xiao P, Tian W, Zhang J (2018) Novel thermoplastic cellulose esters containing
584 bulky moieties and soft segments. ACS Sustainable Chem Eng 6: 4931−4939.
585 https://doi.org/10.1021/acssuschemeng.7b04466
586 Edgar K J, Buchanan C M, Debenham J S, Rundquist P A, Seiler B D, Shelton M C, Tindall D
587 (2001) Advances in cellulose ester performance and application. Prog Polym Sci 26:
588 1605−1688. https://doi.org/10.1016/S0079-6700(01)00027-2
589 El Seoud O A, Marson G A, Ciacco G T, Frollini E (2000) An efficient, one-pot acylation of
590 cellulose under homogeneous reaction conditions. Macromol Chem Phys 201: 882–889.
591 https://doi.org/10.1002/(SICI)1521-3935(20000501)201:8<882::AID-MACP882>3.0.CO;2-I
592 Fan G, Wang M, Liao C, Fang T, Li J, Zhou R (2013) Isolation of cellulose from rice straw and its
593 conversion into cellulose acetate catalyzed by phosphotungstic acid. Carbohydr Polym 94:
594 71–76. https://doi.org/10.1016/j.carbpol.2013.01.073
595 Geng Y, Xiong S, Li B, Liao Y, Xiao X, Yang S (2018) $H_3PW_{12}O_{40}$ grafted on CeO_2: a high-
596 performance catalyst for the selective catalytic reduction of NO_x with NH_3. Ind Eng Chem
597 Res 57: 856–866. https://doi.org/10.1021/acs.iecr.7b03947
598 Heinze T, Dicke R, Koschella A, Kull A H, Klohr E, Koch W (2000) Effective preparation of
599 cellulose derivatives in a new simple cellulose solvent. Macromol Chem Phys 201: 627–631.
600 https://doi.org/10.1002/(SICI)1521-3935(20000301)201:6<627::AID-MACP627>3.0.CO;2-Y
601 Heinze T, Liebert T (2001) Unconventional methods in cellulose functionalization. Prog Polym
602 Sci 26: 1689–1762. https://doi.org/10.1016/S0079-6700(01)00022-3
603 Hussain M A, Liebert T, Heinze T (2004) Acylation of cellulose with *N,N′*-carbonyldiimidazole-
604 activated acids in the novel solvent dimethyl sulfoxide/tetrabutylammonium fluoride.
605 Macromol Rapid Commun 25: 916–920. https://doi.org/10.1002/marc.200300308
606 Huang K, Wang B, Cao Y, Li H, Wang J, Lin W, Mu C, Liao D (2011) Homogeneous preparation
607 of cellulose acetate propionate (CAP) and cellulose acetate butyrate (CAB) from sugarcane
608 bagasse cellulose in ionic liquid. J Agric Food Chem 59: 5376–5381.
609 https://doi.org/10.1021/jf104881f
610 Hu J, Wu Q, Li W, Ma L, Su F, Guo Y, Qiu Y (2011) Epoxidation of alkenes catalyzed by phenyl
611 group-modified, periodic mesoporous organosilica-entrapped, dimeric manganese-salen
612 complexes. ChemSusChem 4: 1813–1822. https://doi.org/10.1002/cssc.201100382
613 Inagaki S, Guan S, Fukushima Y, Ohsuna T, Terasaki O (1999) Novel mesoporous materials with
614 a uniform distribution of organic groups and inorganic oxide in their frameworks. J Am
615 Chem Soc 121: 9611–9614. https://doi.org/10.1021/ja9916658
616 Inagaki S, Guan S, Ohsuna T, Terasak O (2002) An ordered mesoporous organosilica hybrid
617 material with a crystal-like wall structure. Nature 416: 304–307.
618 https://doi.org/10.1038/416304a
619 Köhler S, Heinze T (2007) Efficient synthesis of cellulose furoates in 1-*N*-butyl-3-
620 methylimidazolium chloride. Cellulose 14: 489–495. https://doi.org/10.1007/s10570-007-
621 9138-8
622 Klemm D, Heublein B, Fink H, Bohn A (2005) Cellulose: fascinating biopolymer and sustainable
623 raw material. Angew Chem Int Ed 44: 3358–3393. https://doi.org/10.1002/anie.200460587

Kuzminska M, Kovalchuk T V, Backov R, Gaigneaux E M (2014) Immobilizing heteropolyacids on zirconia-modified silica as catalysts for oleochemistry transesterification and esterification reactions. J Catal 320: 1–8. https://doi.org/10.1016/j.jcat.2014.09.016

Kozhevnikov I V, Kloetstra K R, Sinnema A, Zandbergen H W, Vanbekkum H (1996) Study of catalysts comprising heteropoly acid $H_3PW_{12}O_{40}$ supported on MCM-41 molecular sieve and amorphous silica. J Mol Catal A 114: 287–298. https://doi.org/10.1016/S1381-1169(96)00328-7

Kasztelan S, Payen E, Moffat J B (1990) The existence and stability of the silica-supported 12-molybdophosphoric acid Keggin unit as shown by Raman, XPS, and ^{31}P NMR spectroscopic studies. J Catal 125: 45–53. https://doi.org/10.1016/0021-9517(90)90076-V

Lefebvre F (1992) ^{31}P MAS NMR study of $H_3PW_{12}O_{40}$ supported on silica: formation of $(\equiv SiOH_2^+)(H_2PW_{12}O_{40}^-)$. J Chem Soc Chem Commun 756–757. https://doi.org/10.1039/C39920000756

Li J, Li D, Xie J, Liu Y, Guo Z, Wang Q, Lyu Y, Zhou Y, Wang J (2016) Pyrazinium polyoxometalate tetrakaidecahedron-like crystals esterify oleic acid with equimolar methanol at room temperature. J Catal 339: 123–134. https://doi.org/10.1016/j.jcat.2016.03.036

Li X, Wang K, Helmer B, Chung T (2012) Thin-film composite membranes and formation mechanism of thin-film layers on hydrophilic cellulose acetate propionate substrates for forward osmosis processes. Ind Eng Chem Res 51: 10039–10050. https://doi.org/10.1021/ie2027052

Li T, Wang Z, Chen W, Miras H N, Song Y-F (2017) Rational design of a polyoxometalate intercalated layered double hydroxide: highly efficient catalytic epoxidation of allylic alcohols under mild and solvent-free conditions. Chem Eur J 23: 1069–1077. https://doi.org/10.1002/chem.201604180

Meng C, Cao G, Li X, Yan Y, Zhao E, Hou L, Shi H (2017) Structure of the SO_4^{2-}/TiO_2 solid acid catalyst and its catalytic activity in cellulose acetylation. React Kinet Mech Catal 121: 719–734. https://doi.org/10.1007/s11144-017-1165-3

Marson G A, El Seoud O A (1999) A novel, efficient procedure for acylation of cellulose under homogeneous solution conditions. J Appl Polym Sci 74: 1355–1360. https://doi.org/10.1002/(SICI)1097-4628(19991107)74:6<1355::AID-APP5>3.0.CO;2-M

Omwoma S, Chen W, Tsunashima R, Song Y-F (2014) Recent advances on polyoxometalates intercalated layered double hydroxides: from synthetic approaches to functional material applications. Coord Chem Rev 258–259: 58–71. https://doi.org/10.1016/j.ccr.2013.08.039

Song D, An S, Sun Y, Guo Y (2016) Efficient conversion of levulinic acid or furfuryl alcohol into alkyl levulinates catalyzed by heteropoly acid and ZrO_2 bifunctionalized organosilica nanotubes. J Catal 333: 184–199. https://doi.org/10.1016/j.jcat.2015.10.018

Schnee J, Eggermont A, Gaigneaux E M (2017) Boron nitride: a support for highly active heteropolyacids in the methanol-to-DME reaction. ACS Catal 7: 4011−4017. https://doi.org/10.1021/acscatal.7b00808

Su F, Guo Y (2014) Advancements in solid acid catalysts for biodiesel production. Green Chem 16: 2934–2957. https://doi.org/10.1039/C3GC42333F

Shi Y, Guo Z, Wang Q, Zhang L, Li J, Zhou Y, Wang J (2017) Amphiphilic mesoporous poly(ionic liquid) immobilized heteropolyanions towards the efficient heterogeneous epoxidation of alkenes with stoichiometric hydrogen peroxide. ChemCatChem 9: 4426–4436. https://doi.org/10.1002/cctc.201700906

Song Y-F, Tsunashima R (2012) Recent advances on polyoxometalate-based molecular and composite materials. Chem Soc Rev 41: 7384–7402. https://doi.org/10.1039/C2CS35143A

Tao M, Sun N, Li Y, Tong T, Wielicako M, Wang S, Wang X (2017) Heteropolyacids embedded in a lipid bilayer covalently bonded to graphene oxide for the facile one-pot conversion of glycerol to lactic acid. J Mater Chem A 5: 8325–8333. https://doi.org/10.1039/C7TA01334E

Tao M, Yi X, Delidovich I, Palkovits R, Shi J, Wang X (2015) Hetropolyacid-catalyzed oxidation of glycerol into lactic acid under mild base-free conditions. ChemSusChem 8: 4195–4201. https://doi.org/10.1002/cssc.201501200

Wu J, Zhang J, Zhang H, He J S, Ren Q, Guo M L (2004) Homogeneous acetylation of cellulose in a new ionic liquid. Biomacromolecules 5: 266–268. https://doi.org/10.1021/bm034398d

Xu Q, Song L, Zhang L, Hu G, Chen Q, Liu E, Liu Y, Zheng Q, Xie H, Li N (2018) Synthesis of cellulose acetate propionate and cellulose acetate butyrate in a CO_2/DBU/DMSO system. Cellulose 25: 205–216. https://doi.org/10.1007/s10570-017-1539-8

Yan L, Li W, Qi Z, Liu S (2006) Solvent-free synthesis of cellulose acetate by solid superacid catalysis. J Polym Res 13: 375–378. https://doi.org/10.1007/s10965-006-9054-x

Yu Y, Miao J, Jiang Z, Sun H, Zhang L (2016) Cellulose esters synthesized using a tetrabutylammonium acetate and dimethylsulfoxide solvent system. Appl Phys A 122: 656. https://doi.org/10.1007/s00339-016-0205-6

Yan H, Yang Y, Tong D, Xiang X, Hu C (2009) Catalytic conversion of glucose to 5-hydroxymethylfurfural over SO_4^{2-}/ZrO_2 and SO_4^{2-}/ZrO_2-Al_2O_3 solid acid catalysts. Catal Commun 10: 1558–1563. https://doi.org/10.1016/j.catcom.2009.04.020

Zhang Y, Chen X, Li L, Chen W, Miras N H, Song Y-F (2019) Mesoporous polymer loading heteropolyacid catalysts: one-step strategy to manufacture high value-added cellulose acetate propionate. ACS Sustainable Chem Eng 7: 4975–4982. https://doi.org/10.1021/acssuschemeng.8b05627

Zhu F, Wang W, Li H (2011) Water-medium and solvent-free organic reactions over a bifunctional catalyst with Au nanoparticles covalently bonded to HS/SO_3H functionalized periodic mesoporous organosilica. J Am Chem Soc 133: 11632–11640. https://doi.org/10.1021/ja203450g

Zhang X, Zhao Y, Xu S, Yang Y, Liu J, Wei Y, Yang Q (2014) Polystyrene sulphonic acid resins with enhanced acid strength via macromolecular self-assembly within confined nanospace. Nature Commun 5: 3170. https://doi.org/10.1038/ncomms4170